IEEE Access
Multidisciplinary | Rapid Review | Open Access Journal

Received January 23, 2021, accepted February 4, 2021, date of publication February 12, 2021, date of current version February 26, 2021.

Digital Object Identifier 10.1109/ACCESS.2021.3058951

Inertia Emulation Through Supercapacitor for a Weak Grid

RATNAM KAMALA SAROJINI AND PALANISAMY KALIANNAN, (Senior Member, IEEE)
School of Electrical Engineering, Vellore Institute of Technology, Vellore 632014, India

Corresponding author: Palanisamy Kaliannan (kpalanisamy@vit.ac.in)

This work was supported by the "Fund for Improvement of S&T infrastructure in universities & higher educational institutions (FIST)" of the Department of Science & Technology (DST) - Government of India for sanctioning and funding the Project to establish the PHIL / HIL set up under Grant SR/FST/ETI-420/2016(C).

ABSTRACT Renewable energy sources (RES) have been widely incorporated into the power generation to offset fossil fuels in order to minimize carbon emissions. Typically, RES based power generation integrated into the power grid through the power electronic converters. These power electronic converters decouple the source from the load without providing inertia. As a result, inertia of the power grid decreases, resulting in undesirable load shedding and cascading failures under power imbalances. In order to preserve stability during contingency events, it is important to add inertia support to the grid. This article demonstrates inertia emulation from the supercapacitor (SC) to resolve the low-inertia issue. Inertia emulator based on supercapacitor (IESC) is formulated to generate inertial power by proportionally linking the grid frequency to the active power reference of SC. This article proposes an enhanced emulated inertia control (EIC) technique based on the frequency deviation and frequency derivative to address low inertia. EIC technique controls the inverter associated with IESC to exhibit the equivalent inertia characteristics as the synchronous generator. Further, the selection of the capacitance value of SC is derived to achieve the required inertia constant. The small-signal stability of IESC is demonstrated using the power angle curve. Further, the stability of the EIC is verified through bode plot. Simulation and hardware-in-loop (HIL) results are provided to verify the effectiveness of EIC employed IESC in a weak grid.

INDEX TERMS Frequency, low-inertia power system, renewable energy sources, supercapacitor.

I. INTRODUCTION

The electricity generation from renewable energy sources (RES) has dramatically increased to reduce carbon emissions and enhance energy sustainability [1]. The RES like solar and wind are connected to the grid through the power electronic converters. The power electronic converters decouple the source from the load. The increase in the power electronic converter-based RES power generation retains low or no inertia. Consequently, the stability of the power grid is starting to decrease due to the reduction in inertia. In conventional power systems, the kinetic energy stored in the synchronous generator (SG) is responsible for counteracting the power imbalances through inertial response. The SG injects/absorbs the active power when power imbalance occurs through inertial response to regulate the frequency [2]. However, the low inertia in power system leads to large frequency deviations and high rate of change of frequency (ROCOF) under frequency events. This situation may lead to load shedding, protective relay tripping and cascading failure [3], [4].

Numerous methods have also been suggested in the literature to address the low inertia problem in the power grid. One basic solution is to increase the ROCOF standards to avoid the tripping of the generator under frequency events [5]. Increasing the ROCOF standard requires a generator test that involves high costs. Another potential solution to tackle the low inertia issue is to use synchronous condensers in the system [6]. Though, the usage of the synchronous condenser is limited by its high installation cost.

In the literature, numerous emulated inertia control (EIC) techniques have been recommended for power electronic converters to replicate the SG inertial characteristics [7], [8]. An emerging control technique to regulate the frequency

The associate editor coordinating the review of this manuscript and approving it for publication was Sanjeevikumar Padmanaban.

in low inertia power systems is known as EIC. In [7], the complete mathematical model of the SG is taken to construct the EIC in the stand-alone microgrid and the controller resulting in numerical instability. EIC technique applied to the PV inverter based on the swing equation is investigated in [8]. In [9], the synchronverter is designed to emulate the inertia of SG using the first-order mathematical model of SG. In [10], the second-order SG model is considered to design the control algorithm; even though the calculation of ROCOF leads to complexity in the algorithm. The EIC control scheme is an appropriate solution for the low inertia power system. The EIC mimics the SG characteristics by regulating the switching pattern of the inverter to offer the inertia and decrease frequency nadir and lower the ROCOF during disturbances. In [11], the small-signal modelling of EIC with ideal grid-connected inverter is analyzed. However, earlier works on EIC only stressed the configuration of the controller and barely addressed the functional use of EICs.

Wind turbines (WT) offer kinetic energy in their spinning masses analogous to SG. Though WT is associated with the grid through a power electronic converter, these spinning masses dissociate from frequency [12]. Typically, WT does not provide inertia support to the grid. In [13], [14] a synthetic inertia control technique is used at the power converter of WT to extract the kinetic energy accumulated in the rotor of WT to provide an inertial response to the grid. In [15], the required inertial power is estimated with the frequency deviation only. In [16], supercapacitor (SC) is attached to the DC-bus to enable the inertial response feature to the WT. In [17], the authors explored a feature of ancillary inertial service for a single-phase rooftop system using battery and SC.

In [18]–[20], the authors investigated the inertial response from the battery. However, the use of low-energy-density batteries for compensating sudden disturbances impacts the life of the battery. Moreover, the usage of SC in the inertial response is acceptable. Only frequency deviation is taken into account to estimate the inertial power, and it is supplied by the SC in [16], [21]. However, both frequency deviation and ROCOF must be included in inertial power estimation to improve the inertia of the grid.

Hence, this article proposes an installation of IESC to solve the low inertia issues in weak grid. The SC is connected to a DC bus through a bi-directional converter to step up the voltage. A three-phase inverter is attached to SC connect to the grid. This article recommends an EIC technique for the three-phase inverter at SC that comprises both the frequency deviation and ROCOF to estimate the necessary inertial power. The estimated inertia by the suggested EIC in this article is explicit, and the SC handles it. The fundamental principle lies in proposed EIC: proportionally linking the ROCOF and frequency deviation to the active power reference of the SC. The DC voltage control is proposed for the bi-directional converter of SC in this article is to link the grid frequency appropriately to the DC bus voltage of SC converter.

The major contributions of the article are summarized here: 1) This article proposes an enhanced EIC technique based on the frequency deviation and frequency derivative terms to address low inertia issue. 2) The correlation between the frequency and DC bus voltage of SC is modelled in DC voltage control of SC to suppress the frequency peak in the recovery process. 3) The required inertial power calculated based on the frequency is delivered through SC with the proposed DC voltage control.

The rest of this article is structured as follows: Section 2 describes the system configuration and modelling of each component in the system, section 3 discusses the use of SC in inertial response, control diagram of EIC and DC voltage control of SC are discussed in section 4, small-signal stability analysis of the proposed IESC is described in section 5, simulation results for the proposed IESC are discussed in section 6, hardware-in-loop (HIL) results are discussed in section 7. Finally, section 8 concludes the contribution of this article.

II. SYSTEM CONFIGURATION

Figure 1 details the schematic diagram of a proposed grid-connected PV system along with inertia equipped with IESC system. The PV fed boost converter is connected to the grid through an inverter 1 and LCL filter. The LCL filter is modelled to filter out the higher-order harmonics to retain overall harmonic distortion within an acceptable range. The ripple current and operating voltage are taken into account when choosing the filter values. The PV based three-phase inverter connected to the grid as a grid feeding inverter. In order to preserve stability under imbalances, it is essential to improve the inertia of the current power grid.

The SC is connected to the DC bus through a bi-directional converter. The bi-directional converter works in two modes. 1) charging mode during the frequency peaks. 2) discharging mode in frequency dips. SC is connected the PCC through an inverter 2 and LCL filter. inverter 1 is controlled with a current controller while the inverter 2 is employed with EIC control to emulate the inertial response. The EIC control at the inverter 2 aims to regulate the load angle for sudden frequency variations. The voltage control loop of bi-directional dc to dc converter aims to regulate the DC bus voltage of the SC, following with its reference. In addition, bi-directional dc to dc converter aims to regulate the frequency of the grid under disturbances. The control at the bi-directional dc to dc converter is designed in such a way that to link the grid frequency variations to the SC voltage. The presented system is effective in supplying inertia under sudden power imbalances. The rest of this section detailed the modelling of each component in the system and briefly explain about the inertia of the power system.

A. PV SYSTEM MODELLING

In PV modelling, the PV cell model considers vital because the PV system performance primarily depends on the accurate cell characteristics [22]. In order to determine the cell

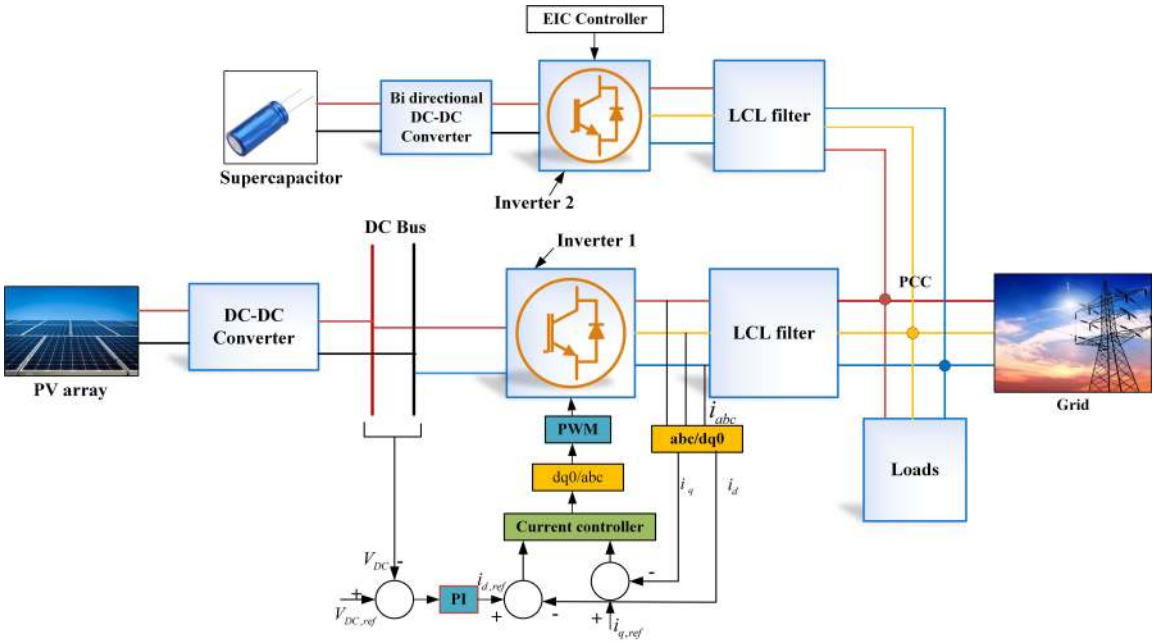

FIGURE 1. Proposed grid-connected PV and inertia equipped with SC system.

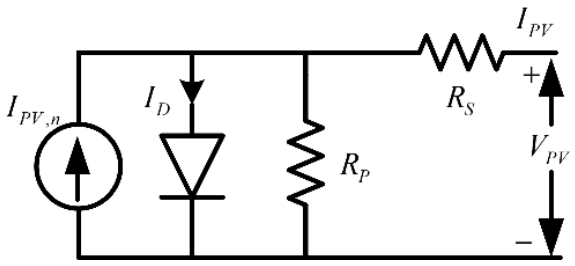

FIGURE 2. Schematic of the single-diode solar PV model.

characteristics, there are two primary modelling approaches: 1) a single-diode model and 2) two-diode model. In this article, the authors used the single diode model to reduce the ambiguity. The schematic diagram of the single-diode model is shown in Figure 2. Generally, the power generation from the PV module is dependent on the temperature and irradiance. The nonlinear electrical characteristics of PV array depends on series resistance (R_S) and parallel resistance (R_P).

The output equation of the solar PV cell from Figure 2 is given as:

$$I_{PV} = I_{PV,n} - \left(I_o\left(e^{V_D/aV_T} - 1\right)\right) - \frac{V_{PV} + I_{PV}R_S}{R_P} \quad (1)$$

Here, $I_{PV,n}$ represents the PV array current, R_S and R_P indicate the series and parallel resistance. I_D denotes the diode current, I_o is the reverse saturation current, V_D is the diode voltage, V_T is the thermal voltage of the diode and it is given as

$$V_T = \frac{N_S kT}{q} \quad (2)$$

Here, N_S is the series-connected cells, k is the Boltzmann constant, T is the temperature. Hence, the solar PV module current can be determined as:

$$I_{PV} = N_{PP}\left\{I_{PV,n} - I_o\left[\exp\left(\frac{V_{PV} + I_{PV}R_S}{V_T N_{SS}}\right) - 1\right]\right\} - \left(\frac{V_{PV} + I_{PV}R_S}{R_p}\right) \quad (3)$$

The PV power is fed to the DC bus through a boost converter which works on the maximum power point tracking algorithm to exploit the maximum power from the PV system. In this article, perturbed and observe maximum power point tracking algorithm is used to extract the maximum power from the PV system. The perturbed and observe algorithm modifies the voltage and calculates the change in power; if the change in power is not zero then the voltage modifies further.

B. MODELLING OF SUPERCAPACITOR

Supercapacitors are electrical energy storage devices that provide high power density. The SC storage technology is used to offer inertial support because it has fast response time, high-power density, and larger cycle life. The ability to choose a supercapacitor device depends on the appropriate power level, voltage rating and interval of the transient power supply. The SC value can be chosen based on the maximum power need to be delivered, and the duration of the time delivered in the inertial response. The nominal voltage of the SC unit is known to be 220 V, and DC bus voltage is 500 V. Time interval considered for the inertial response

is one minute. The energy balancing of SC can be known as

$$\frac{1}{2}C_{SC}V_{SC}^2 = P_{SC}t_{Iner} \tag{4}$$

where,C_{SC} is the capacitance of SC, V_{SC} is the SC voltage, P_{SC} is the required power rating and t_{Iner} is the duration of inertial response.

C. GRID MODELLING

In this article, the grid is considered to be a weak grid; Usually, the strength of the grid is assessed by the short circuit ratio (SCR).

$$SCR = \frac{1}{Z_g(\mathrm{p}\cdot\mathrm{u})} \tag{5}$$

The SCR value is more than 3 for strong grids, SCR value for a weak grid is between 2 to 3, and the SCR value for a very weak grid is less than 2. In this article, the SCR value is chosen between 2 and 3.

D. VARIABLE LOCAL LOAD SYSTEM AT PCC

In the real power grid, load fluctuates continuously. Thus, in this work, demand is varied at a certain time. The load at the PCC consists of two loads. Out of which two loads one load is constant, and another load is a variable load operating at a particular time period.

E. INERTIA OF THE POWER SYSTEM

The inertia of the power system is extracted from the kinetic energy stored in the rotating parts of the traditional power systems. The kinetic energy of these massive rotating machines acts as a shock absorber to prevent grid frequency from falling too quickly when demand exceeds supply or rising too fast when supply exceeds demand. Without this stabilizing force (inertia), power grids might face a higher chance of frequency excursions that forcing generators offline or trigger cascading outages.

The kinetic energy (E_{KE}) can be expressed as

$$E_{KE} = \frac{1}{2}J\omega^2 \tag{6}$$

where, J is the moment of inertia of rotor, ω is the synchronous speed. The inertia constant (H) of a single machine can be defined in (7) as the ratio of the kinetic energy to the rated power capacity (S).

$$H = \frac{\frac{1}{2}J\omega^2}{S} \tag{7}$$

The total inertia constant of the power system containing 'n' machines can be obtained as

$$H_{\mathrm{Total}} = H_1 + H_2 + \ldots\ldots + H_n \tag{8}$$

It is clear from (7) that the inertia of the system is proportional to the kinetic energy of the rotating machine. However, the increase in power generation from power-electronic based PV system significantly reduces the inertia.

TABLE 1. Correspondence Between IESC and SG.

IESC	Traditional SG
Capacitance of SC	Inertia of rotor
Filter	Stator of the SG
SC voltage	Rotor speed
Output voltage of the inverter	SG internal voltage
Output voltage of the filter	Terminal voltage of SG
Energy stored in SC	Energy stored in rotor

The PV system is typically configured to inject power to the grid but not to store energy. Whereas SC is the static energy storage device. It has low-energy density and high-power density. This attribute allows the SC to be used in inertia applications. In order to improve inertia, it is also important to expand the inertia support from rotating parts to the static SC.

III. SUPERCAPACITOR FOR INERTIA APPLICATION

The capacitance (C_{SC}) of a SC can be known by its charging/discharging rate and the voltage across (V_{SC}) the device [16]. The comparison of emulated inertia control with inverter and SG is presented in [23]. Inertia emulated by the SC is analogous to inertia of the rotor of traditional SG. Even though the SC is static device, it has a high-power density. With EIC technique applied at inverter of IESC, it can support the active power in inertial response. With a proper EIC technique at inverter at SC and DC voltage control at the bi-directional converter at the SC can exchange the energy at the power grid under power imbalance. Theoretically, SC is capable of imitating the rotational inertia of SG.

The inertia J of a SG depends on the rotor structure. Similarly, the capacitance of the SC is static irrespective of the charges inside. From the point of view of energy transfer, rotor and SC act as power transmitter that transports the power under disturbances. Table 1 summarises equivalence between the IESC and SG. The energy stored in the SC can be estimated as

$$E_{SC} = \frac{1}{2}C_{SC}V_{SC}^2 \tag{9}$$

It can be found that the ω in (1) is identical to V_{SC} in (4).

It is clearly shown that from (6) and (9), the energy stored in the SG rotor is proportional to the square of the synchronous frequency. Similarly, the energy stored in the SC is proportional to the square of SC voltage.

The SC is able to respond to frequency changes in the weak grid and able to emulate the inertia constant H_{SC}. The rest of the section detailed the SC sizing to provide the inertia. The energy stored in the SC is discharged/charged for injecting/absorbing the active power to support frequency regulation. A comparison can be found between the energy stored in SC and the kinetic energy stored in the rotor of SG.

The swing equation for the rotor of SG after an imbalance can be expressed as:

$$\frac{2H_{SC}}{\omega_{g0}}\frac{d\omega_g}{dt} = \Delta P \tag{10}$$

where H_{SC} refers to the inertia constant, ω_{g0} is the nominal angular frequency of the grid, ΔP is the power imbalance. The energy stored in the SC can be retrieved by varying the SC voltage. The electrical characteristics of the SC under power imbalance is known as:

$$\frac{C_{SC}V_{SC}}{S_{PV}}\frac{dV_{SC}}{dt} = \Delta P \tag{11}$$

where C_{SC} is the capacitance of the SC, V_{SC} is the SC voltage, S_{PV} is the capacity of the PV system. To assign the inertia constant for the SC with both the power imbalances in (10) and (11) are equated.

$$\frac{2H_{SC}}{\omega_{g0}}\frac{d\omega_g}{dt} = \frac{C_{SC}V_{SC}}{S_{PV}}\frac{dV_{SC}}{dt} \tag{12}$$

After integrating on both sides of (12):

$$\frac{2H_{SC}}{\omega_{g0}}\omega_g = \frac{C_{SC}V_{SC}^2}{2S_{PV}} + K_1 \tag{13}$$

where K_1 is the integration constant $= 2H_{SC} - \frac{C_{SC}V_{SC0}^2}{2S_{PV}}$ Hence, the inertia constant realized from the SC can be written as:

$$H_{SC} = \frac{C_{SC}\omega_{g_0}V_{SC0}\Delta V_{SC,\max}}{2S_{PV}\Delta\omega_{g,\max}} \tag{14}$$

where $\Delta V_{SC,\max}$ is the maximum allowed SC voltage variation, $\Delta\omega_{g,\max}$ maximum allowed grid frequency variation. From (14), the inertia coefficient depends on the following factors: the capacitance of the SC, the rated voltage of SC, the maximum allowable variation of the SC voltage and the maximum allowable frequency variation. In this article maximum allowable variation in frequency is set as 0.25 Hz; the maximum allowable variation of the SC voltage is considered as 40V. The characteristics of inertia constant (H_{SC}) are depicted in Figure 3. As can be seen, the value is enhanced by the increment of both SC voltage and SC value. It is worth noting that, even under the operation of normalization, the SC voltage change can contribute more to the inertia increase in allowable regions.

IV. CONTROL SCHEMATIC FOR IESC

As stated earlier, SC does not have that capacity to automatically release /absorb the power in frequency disturbances like SG. Hence, a suitable controller needs to be designed to derive the energy from SC in frequency events. IESC system requires two control techniques to satisfy the inertia requirement. EIC technique at the inverter of IESC (inverter 2 in Figure 1) is designed to extract/store the energy from/in SC to arrest the frequency change during power imbalances. The DC voltage control technique at the bi-directional converter of SC links the DC bus voltage and frequency appropriately.

The proposed EIC presented in this article consists of two control loops. The main aim of the first loop to measure the required inertial power to minimize the ROCOF. Whereas, the second loop intended to calculate the required power to arrest

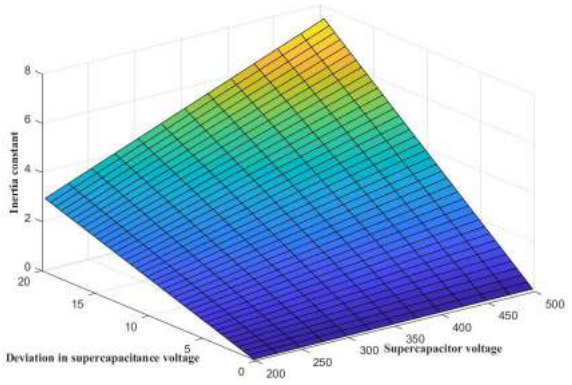

FIGURE 3. Variation of inertia constant (H_{SC}) with SC voltage (V_{SC}) and SC capacitance voltage deviation value.

the frequency deviation. Whenever grid frequency changes from the nominal value, the inertial power command is triggered to vary the load angle of IESC. As per the Figure 4, the ROCOF signal is measured and filtered by a low pass filter to eliminate the measurement noise in the first loop. Then, a dead band (± 0.015 Hz) is deployed to avoid the participation of inertia control on a small frequency variation, resulting in heavy power pulsations of SC in the normal operating condition. In the second loop, the grid frequency deviation is measured and filtered by a low pass filter to eliminate the measurement noise.

The inertial power (P_{Inertia}) signal required to mitigate the frequency deviations is applied for the EIC technique to alter the load angle of inverter 2. Depends on the load angle the switching pattern of the inverter 2 is changed.

Hence, the required inertial active power calculated based on the Figure 4 is:

$$P_{\text{Inertia}} = K_D\Delta f + K_I\frac{df}{dt} \tag{15}$$

where K_D is the damping constant and K_I is the inertia constant.

It is essential to select appropriate values of K_D and K_I. Otherwise, it may cause poor performance of the controller. The inertial constant is proportional to ROCOF. A high K_I value may result in over-charging and discharging of SC. K_D is the gain of frequency deviation control loop; a high K_D selection may lead to a large drop in SC voltage. K_D is selected based on the droop characteristics of SG (from 2%-12%).

An optimal combination of the two gains can achieve good performance of proposed EIC technique on the frequency stability improvement. A ramp rate limit (± 0.5 pu/s) is added to prevent the immediate on/off activated signal in case reaching the minimum SC voltage. A proper value of the ramp rate limit makes the transfer period smoother and less stress on the SC. The estimated inertial power signal from Figure 4 is connected to the proposed EIC, as shown in Figure 5. The EIC technique alters the load angle of the IESC to inject/absorb the power to/from the grid.

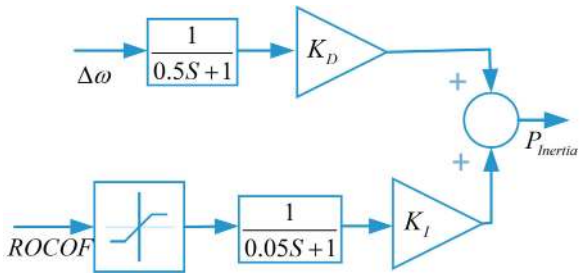

FIGURE 4. The required inertial power calculation block.

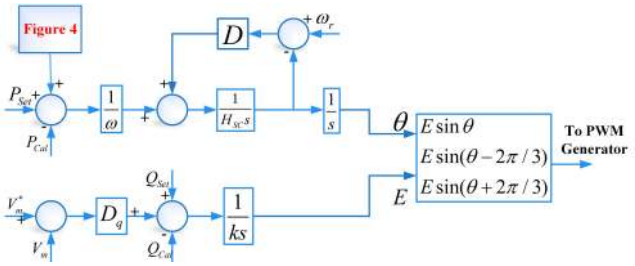

FIGURE 5. Proposed emulated inertia control.

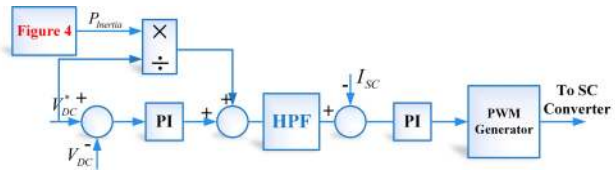

FIGURE 6. DC voltage control of SC.

The DC voltage control of SC bi-directional converter is shown in Figure 6. The reference SC current is calculated based to pump the required inertial power into the grid under frequency deviations. After calculating the reference SC current, the highly varying component is separated by using the high pass filter and supplied/absorbed by the SC.

V. SMALL-SIGNAL STABILITY ANALYSIS OF IESC

The effect of low inertia on the small-signal stability of the system is studied in this section. The small-signal stability studies involve assessing whether or not synchronism is preserved after the machine has been subjected to disturbance. The equal-area criterion used for a quick prediction of stability in synchronous machines is used here to determine the stability of the grid-connected IESC. The per-phase model of the proposed system in this article is shown in Figure 7. The instantaneous active power from the SC inverter is given as:

$$P_{SC} = \frac{EV_g}{X}\sin(\theta) \tag{16}$$

Based on the simplified model, Figure 7 shows the power angle curve for the small frequency deviations. The output power P_{sc} equates to P_{Inertia} under power imbalances. Therefore, the output power P_{SC} equates the required inertial power P_{Inertia} as shown in Figure. 8 (a). Two operating points a and b are existing to meet the required inertial power.

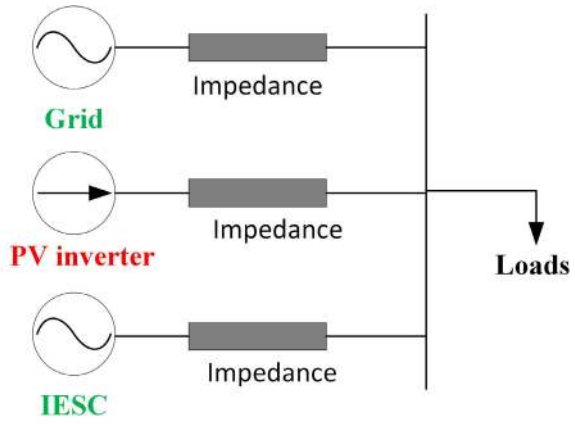

FIGURE 7. Single line diagram of the proposed system.

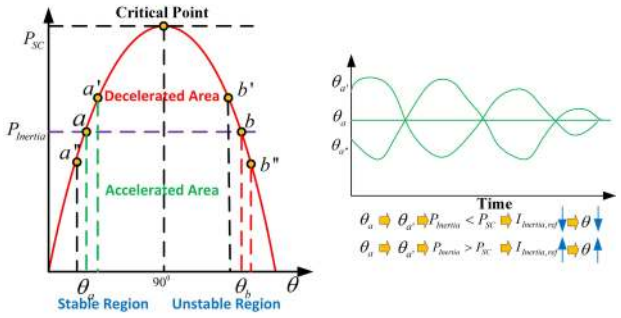

FIGURE 8. Illustration of IESC small-signal stability (a) Power angle curve (b) Stable response at point a.

Under frequency fluctuations, to meet the required inertia power (P_{Inertia}), there are two equilibrium points a and b. However, the operating point a is able to operate in a stable condition, whereas the operating point b is unstable.

A. AT POINT A

After the frequency event, the required inertial power (P_{Inertia}) has to be supplied from SC, and the load angle increases to θ_a. The load angle is oscillating between $\theta_{a'}$ and $\theta_{a'}$ before settling to θ_a. The positive deviation $\Delta\theta$ is created when the load angle is reached $\theta_{a'}$. In this case, the SC output is more than the P_{Inertia} then the DC controller at SC bi-directional converter decreases the inertia reference current (I_{Inertia}) and EIC controller at the SC inverter decreases the load angle to return to the equilibrium point a. Similarly, the negative deviation of $\Delta\theta$ is created when the load angle is reached $\theta_{a'}$. In this situation, the output power from SC reference current I_{Inertia} and EIC controller at the SC inverter increases the load angle to return to the equilibrium point a.

B. AT POINT B

The stability at point b is completely different from the point a. Similarly, assuming a positive $\Delta\theta$ is imposed on θ_b, such that θ increases to $\theta_{b'}$. Accordingly, P_{Inertia} is greater than P_{SC}, then the EIC controller increases the load angle

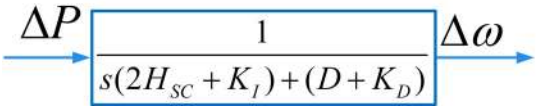

FIGURE 9. Simplified small-signal diagram of EIC.

of the inverter at the SC, and further decreasing the output power P_{SC}. Hence, the load angle of the IESC keep on increasing. Obviously, a positive load angle disturbance will introduce a positive feedback, and thus, non-oscillatory instability. On the contrary, if θ is changed from θ_b to $\theta_{b'}$. with a negative angle disturbance, P_{Inertia} is smaller than P_{SC}, In this case the output from SC is more than P_{Inertia} then DC controller of at SC bi-directional converter decreases the inertia reference current (I_{Inertia}) and EIC controller at the SC inverter decreases the load angle to return to stable operating point a. hence, the operating point b may either loose the stability or regain the stability by moving to point a.

C. STABILITY ANALYSIS OF EIC

Since this article aims to regulate the frequency, the stability analysis of active power loop of the proposed EIC is discussed in this section. The simplified small-signal model of proposed EIC active power control is shown in Figure 9.

The transfer function for the load angle to the active power is known as:

$$G_{P\theta}(s) = \frac{1}{(2H_{SC} + K_I)\,\mathrm{s}^2 + (D + K_D)\,s} \tag{17}$$

Figure 10 shows the bode plot for proposed EIC control for (17). The parameters are tuned to achieve the phase margin of 56 degrees at the infinite gain margin.

The transfer function for the frequency to power can be rewritten from (17) as:

$$G_{p\omega}(s) = \frac{1}{(2H_{SC} + K_I)\,\mathrm{s} + (D + K_D)} \tag{18}$$

The frequency variation created for the power imbalance can be indicated as:

$$|\ \Delta\omega = \frac{1}{(2H_{SC} + K_I)\,\mathrm{s} + (D + K_D)}\Delta P \tag{19}$$

According to initial value theorem, the frequency variation for the step power change can be derived as:

$$\Delta\omega(0) = \lim_{s\to\infty} s\Delta\omega = \frac{\Delta P}{2H_{SC} + K_I} \tag{20}$$

Eq. (20) proved that the initial frequency variation is directly proportional to the power imbalance and inversely proportional to the inertia.

In the same way, from the final value theorem, the steady-state frequency deviation after a step change in power imbalance can be derived as:

$$\Delta\omega(\infty) = \lim_{s\to 0} s\Delta\omega = 0 \tag{21}$$

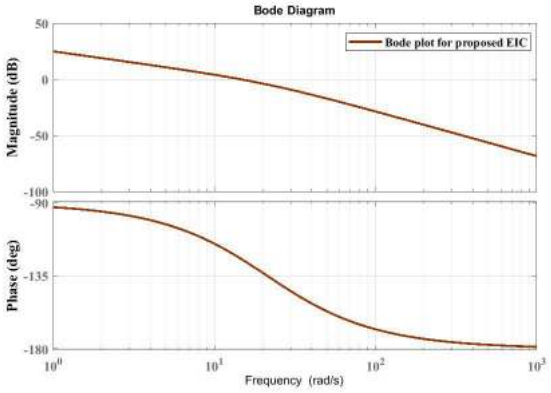

FIGURE 10. Bode plot for proposed EIC.

TABLE 2. Simulation and HIL Parameters.

Parameter	Value
Nominal frequency (f)	50 Hz
Nominal Voltage (V^*)	220 V
Rated DC bus voltage (V_{DC})	500 V
PV cell for both PV arrays	V_{OC}=37.3 V, I_{SC}=8.2 A V_m =30.3 V, I_m=7.5 A N_S=10, N_P=5
Rating of SC	0.8 F,220V
DC bus Capacitor	3300 μF
Inverter side inductance (L_1)	2.1 mH
Load side inductance (L_2)	0.8 mH
Filter capacitance (C)	12 μF
Frequency Drooping Coefficient (D_P)	50
Voltage drooping coefficient (D_q)	120
Gain(k)	1000 A.s
Inertia coefficient (H_{SC})	2.8

From (21), it is clear that the steady-state frequency deviation is zero, and it is independent of the inertia value.

VI. SIMULATION RESULTS

The proposed IESC system is modelled in MATLAB/Simulink and the system parameters are tabulated in Table 2. In this section, the effectiveness of inertia emulation through IESC is analysed in MATLAB simulations. The frequency event is created by step increase in the load. The variation in frequency and inertial power at the frequency event are analysed.

A. SUDDEN INCREASE IN LOAD DEMAND

This section aims to assess the inertia emulation through EIC employed IESC during step increase in load. Initially, the load of 8000 W is considered to be constant applied throughout the simulations. A sudden variation of the load has been modelled at $t = 2$ s to create a power imbalance, and it leads to frequency oscillations. Figure 11 shows that the grid frequency deviation is dropped to 49.78 Hz without any external inertia support to the weak grid. Whereas, the frequency deviation is limited to 49.86 Hz with inertial support from the IESC with the proposed EIC technique. An improvement of 0.08 Hz of

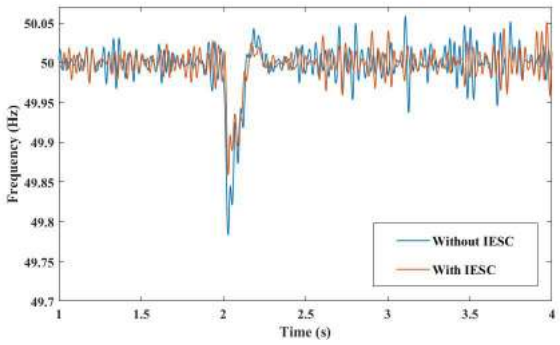

FIGURE 11. Frequency variations for sudden load increase.

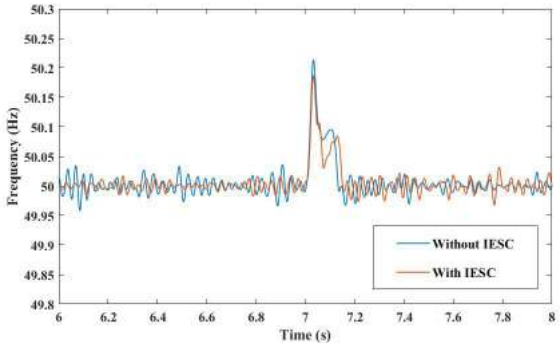

FIGURE 12. Frequency variations for sudden load decrease.

the frequency nadir is observed from Figure 11 when EIC employed IESC is configured in the weak grid. This indicates the advantage of system frequency stability provided by EIC employed IESC. The proposed EIC technique, along with the DC voltage control at IESC, reduces the frequency peak in the recovery process and increases the inertia of the system. The EIC control applied at IESC limits the frequency nadir and reduced the ROCOF without a peak in the recovery process shown in Figure 11.

B. SUDDEN DECREASE IN LOAD DEMAND

This section aims to demonstrate the inertia emulation through IESC when the load decreases. Initially, the load of 8000 W is considered to be constant throughout the simulations. A rapid shift in load was simulated at $t = 7$ s to create a mismatch in generation and demand, leading to frequency oscillations. Figure 12 shows that the frequency of the grid is raised to 50.22 Hz without any additional inertia support to the weak grid. The frequency rise is limited to 50.18 Hz with inertial support from the IESC with the proposed EIC technique. An improvement of 0.04 Hz of the frequency peak is observed from Figure 12 when EIC employed IESC is configured in the weak grid. It indicates the advantage of system frequency stability provided by EIC employed IESC under sudden decrease in load demand. The proposed EIC technique considers both the loops (frequency deviation and ROCOF) to estimate the inertial power to minimize the frequency peak. The proposed EIC technique and the DC voltage

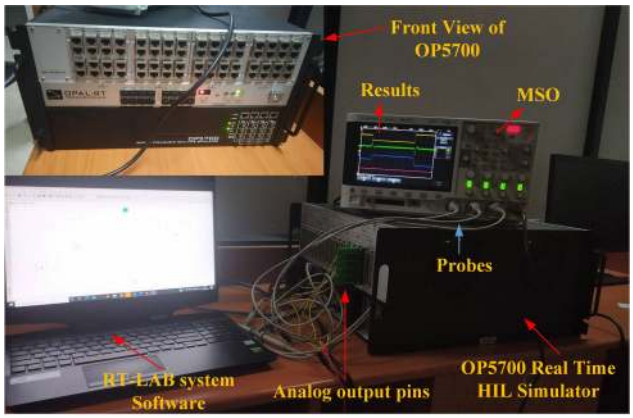

FIGURE 13. HIL setup.

control at IESC, effectively improve the frequency stability under sudden load imbalances.

VII. HIL RESULTS

In order to verify the proposed IESC system for improving inertia of the grid, two scenarios were tested. The first scenario is to validate the performance of IESC in load variations. Whereas, the second scenario is to validate the performance of IESC in PV power variations. The proposed system which is displayed in Figure 1 is loaded into the OP5700 real-time simulator for validation. Figure 10 shows the HIL Setup. The system parameters used in this article for the HIL test is tabulated in Table 2.

A. WITH LOAD TRANSITIONS

This scenario analyses the performance of IESC system connected to the weak grid consists of PV under constant irradiation level with load transitions. The maximum power of 10000 W is extracted from the PV array under standard irradiation level. The constant load of 8000 W is considered at PCC, and the excess power from PV is pumped into the grid. The HIL results for the load transitions are shown in Figure 11. Another load of 4000 W is added at $t = t_1$ s then the frequency is falling from the nominal value. When frequency deviates from the nominal value, the EIC technique activates at IESC system and injects the inertial power to resist the changes in frequency. The inertial power injected into the grid to maintain the frequency is shown in Figure 14(a). The inertial power injected from SC is calculated by the EIC control according to frequency deviation and ROCOF. Depends upon the estimated inertial power, the inertia current at the SC bidirectional current is altered. Figure 14(b) visualises the PV power, variations in load demand, changes in frequency and voltage. The EIC technique resists the frequency nadir to 49.85 Hz under a sudden increase in load demand. At $t = t_2$ s the step decrease in load is created, and it creates the frequency rise. When the frequency is rising from the nominal value, then the EIC activates at IESC and absorbs the extra inertial power. The inertial power is absorbed and stored in SC. The frequency rise is restricted to 50.24 Hz by the EIC control technique

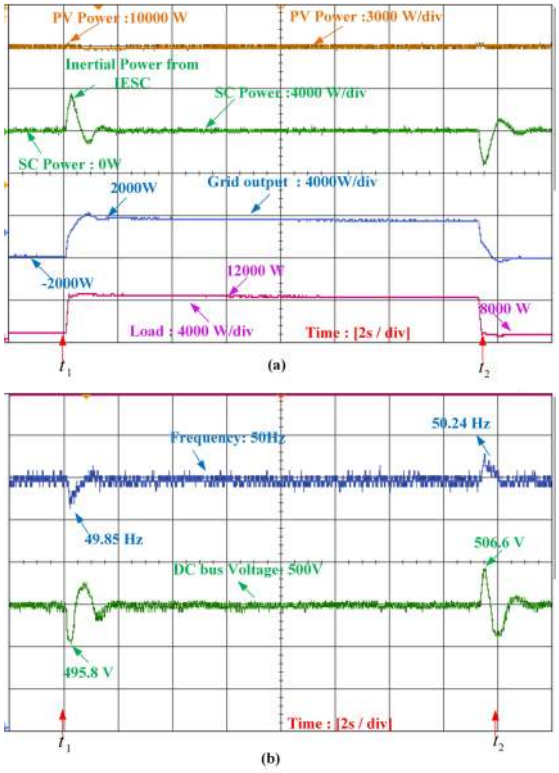

FIGURE 14. (a) Load transition under constant irradiation (a) power from PV-inverter, SC, grid and load; (b) frequency and DC bus voltage.

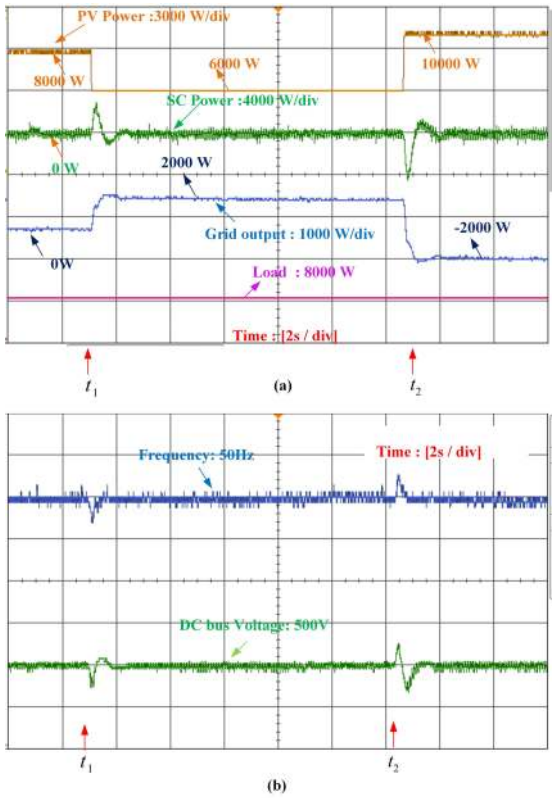

FIGURE 15. Variable irradiation at constant load (a) power from PV-inverter, SC, grid and load; (b) PV power, load, frequency and DC bus voltage.

under sudden load decrease. Hence, the EIC controlled SC resembles the SG inertial characteristics in load variations. The EIC technique alters the load angle to inject/absorb the power under frequency deviations.

B. WITH IRRADIATION TRANSITIONS

This scenario analyses the proposed system under PV irradiation variations. The PV system is operated at an irradiance of 800 W/m^2 and 8000 W power is extracted from PV, and the load estimated at the PCC is 8000 W. The source side variations are created at PV side to create the frequency variations and to test the effectiveness of IESC system. The step changes in PV irradiation are designed at a rate of 600 W/m^2 and 1000 W/m^2 at s and s respectively. The HIL results for changes in irradiation are shown in Figure 15. At $t- = t_1$ s, the PV power generation decreases as the PV irradiation level decreases and it creates the imbalance in power. This situation creates the grid frequency to dip, hence the EIC control at IESC activates to arrest the frequency deviation. When the frequency fall is created, then load angle of the EIC control increases to pump inertial power to the grid. At $t = t_2$ s the PV power generation increases as the PV irradiation level increases to 1000 W/m^2. The power generated by the PV is supplied to the load and the excess power is exported to the grid. The sudden increase in the PV power creates an impact in frequency. When rise in frequency observed, then the EIC control at IESC decreases the load angle to absorb the excess power in inertial response. This transition creates an oscillation in grid frequency and proposed EIC technique able to handle the grid frequency variations under the changes in irradiations also.

VIII. CONCLUSION

This article has been verified the effectiveness of inertia emulation by SC for low inertia systems. Emulated inertia power is realized by associating the grid frequency deviation and ROCOF to the reference voltage of the SC. Energy exchange is takes place through SC under disturbances. Hence, IESC can efficiently improve the power system inertia and frequency regulation. This article proves that three-phase inverter and SG are exhibiting the similar inertial characteristics. The small-signal stability analysis of the IESC system is verified theoretically. The value of supercapacitance is derived for different inertia values. Hardware in loop results have verified the theoretical analysis and the effectiveness of emulated inertia.

The future work focusses on the two topics. First study emphasis on the stability analysis and optimal placement of IESC in the power grid to enhance the inertial response. Second study concentrates on the online estimation of inertia to assess the stability of the grid.

REFERENCES

[1] A. Zervos, "Renewables 2018 global status report," REN21, Paris, France, Global Status Rep., 2018.

[2] K. S. Ratnam, K. Palanisamy, and G. Yang, "Future low-inertia power systems: Requirements, issues, and solutions—A review," *Renew. Sustain. Energy Rev.*, vol. 124, May 2020, Art. no. 109773.
[3] M. G. Kundur, P. Balu, and N. J. Lauby, *Power System Stability and Control*. New York, NY, USA: McGraw-Hill, 1994.
[4] W. Group, "RoCoF modification proposal—TSOs' recommendations," EirGrid SONI, Ireland, Tech. Rep., 2012.
[5] *Inertia and Rate of Change of Frequency (RoCoF)*, Executive Summary, ENTSO-E, Brussels, Belgium, 2020.
[6] H. T. Nguyen, G. Yang, A. H. Nielsen, and P. H. Jensen, "Combination of synchronous condenser and synthetic inertia for frequency stability enhancement in low-inertia systems," *IEEE Trans. Sustain. Energy*, vol. 10, no. 3, pp. 997–1005, Jul. 2019.
[7] R. K. Sarojini and K. Palanisamy, "Emulated inertia control for the standalone microgrid with high penetration of renewable energy sources," *Int. J. Renew. Energy Res.*, vol. 10, no. 2, pp. 831–842, 2020.
[8] P. Rodriguez, C. Citro, J. I. Candela, J. Rocabert, and A. Luna, "Flexible grid connection and islanding of SPC-based PV power converters," *IEEE Trans. Ind. Appl.*, vol. 54, no. 3, pp. 2690–2702, May 2018.
[9] H. Xu, C. Yu, C. Liu, Q. Wang, and X. Zhang, "An improved virtual inertia algorithm of virtual synchronous generator," *J. Modern Power Syst. Clean Energy*, vol. 8, no. 2, pp. 377–386, 2020.
[10] Y. Yoo, S. Jung, and G. Jang, "Dynamic inertia response support by energy storage system with renewable energy integration substation," *J. Modern Power Syst. Clean Energy*, vol. 8, no. 2, pp. 260–266, 2020.
[11] R. K. Sarojini and K. Palanisamy, "Small signal modelling and determination of critical value of inertia for virtual synchronous generator," in *Proc. Innov. Power Adv. Comput. Technol. (i-PACT)*, 2019, pp. 1–6.
[12] G. Shu-Feng, Z. Jie-Tan, A. Philip, H. Li-Li, and J. Jing, "A review of wind turbine deloaded operation techniques for primary frequency control in power system," in *Proc. China Int. Conf. Electr. Distrib. (CICED)*, Sep. 2018, pp. 63–71.
[13] H. T. Nguyen, G. Yang, A. H. Nielsen, and P. H. Jensen, "Frequency stability enhancement for low inertia systems using synthetic inertia of wind power," in *Proc. IEEE Power Energy Soc. Gen. Meeting*, 2017, pp. 1–5.
[14] H. T. Nguyen, M. N. Chleirigh, and G. Yang, "A technical & economic evaluation of inertial response from wind generators and synchronous condensers," *IEEE Access*, vol. 9, pp. 7183–7192, 2021.
[15] D. Gautam, L. Goel, R. Ayyanar, V. Vittal, and T. Harbour, "Control strategy to mitigate the impact of reduced inertia due to doubly fed induction generators on large power systems," *IEEE Trans. Power Syst.*, vol. 26, no. 1, pp. 214–224, Feb. 2011.
[16] J. Zhu, J. Hu, W. Hung, C. Wang, X. Zhang, S. Bu, Q. Li, H. Urdal, and C. D. Booth, "Synthetic inertia control strategy for doubly fed induction generator wind turbine generators using lithium-ion supercapacitors," *IEEE Trans. Energy Convers.*, vol. 33, no. 2, pp. 773–783, Jun. 2018.
[17] R. K. Sarojini, K. Palanisamy, P. Sanjeevikumar, and J. B. Nielsen, "Inertia emulation control technique based frequency control of grid-connected single-phase rooftop photovoltaic system with battery and supercapacitor," *IET Renew. Power Gener.*, vol. 14, no. 7, pp. 1156–1163, May 2020.
[18] F. M. Gonzalez-Longatt and S. M. Alhejaj, "Enabling inertial response in utility-scale battery energy storage system," in *Proc. IEEE Innov. Smart Grid Technol. Asia (ISGT-Asia)*, Nov. 2016, pp. 605–610.
[19] P. V. Brogan, R. J. Best, D. J. Morrow, K. McKinley, and M. L. Kubik, "Effect of BESS response on frequency and RoCoF during underfrequency transients," *IEEE Trans. Power Syst.*, vol. 34, no. 1, pp. 575–583, Jan. 2019.
[20] A. Hosseinipour and H. Hojabri, "Virtual inertia control of PV systems for dynamic performance and damping enhancement of DC microgrids with constant power loads," *IET Renew. Power Gener.*, vol. 12, no. 4, pp. 430–438, Mar. 2018.
[21] R. Zhang, J. Fang, and Y. Tang, "Inertia emulation through supercapacitor energy storage systems," in *Proc. ICPE ECCE Asia 10th Int. Conf. Power Electron. (ECCE Asia)*, vol. 3, 2019, pp. 1365–1370.
[22] J. P. Ram, D. S. Pillai, A. M. Y. M. Ghias, and N. Rajasekar, "Performance enhancement of solar PV systems applying P&O assisted flower pollination algorithm (FPA)," *Sol. Energy*, vol. 199, pp. 214–229, Mar. 2020.
[23] R. K. Sarojini and K. Palanisamy, "Comparison of emulated inertia controller with synchronous generator," in *Proc. IOP Conf., Mater. Sci. Eng.*, 2020, vol. 937, no. 1, Art. no. 012018.

RATNAM KAMALA SAROJINI received the B.Tech. and M.Tech. degrees (Hons.) in electrical engineering from JNTUK, India, in 2010 and 2016, respectively. She is currently pursuing the Ph.D. degree in electrical engineering with the Vellore Institute of Technology, Vellore, India. Her research interests include frequency stability, virtual inertia, and emulated inertia.

PALANISAMY KALIANNAN (Senior Member, IEEE) received the bachelor's degree in electrical engineering from the KSR College of Technology, India, in 2000, the master's degree (Hons.) in applied electronics from the Coimbatore Institute of Technology, India, in 2004, and the Ph.D. degree in electrical engineering from the Vellore Institute of Technology, Vellore, India, in 2013. He has been the Deputy Director of electrical maintenance and projects and an Associate Professor of the Energy and Power Electronics Division, Vellore Institute of Technology, where he has been the Head of the Center for Smart Grid Technology, since 2007. From 2016 to 2018, he was the Head of the Department of Energy and Power Electronics Division. He has authored more than 96 scientific articles in refereed conference proceedings and international journals in the field of renewable energy, battery energy storage, multilevel converters, and power quality. He is a certified Energy Auditor by the Bureau of Energy Efficiency, Government of India. He has taken up various consultancy projects in energy efficiency and power quality improvement.